Numerical simulation of turbulent characteristics (structures and statistics) in channel with periodic two-dimensional ribs

Mehdi Ahmadi [1,*], Behnaz Bagheri Dastgerdi [2]

1. Islamic Azad University, Shahrekord Branch, Ardal Center, Iran
2. Islamic Azad University, Shahrekord Branch, Iran
M_Ahmadi@iaushk.ac.ir , m.behnaz90@gmail.com

Abstract: Numerical simulation of turbulent channel flow with periodic two– dimensional ribs has been performed in order to investigate the turbulent characteristic behind the ribs. The Reynolds numbers based on the friction velocity and the channel half width are 10- 1500. In the wake region, the mean flow becomes asymmetric with respect to the centerline of the geometry through the Coanda effect. Large – scale vortices are generated at the height of the ribs edges. The small – scale vortices are convicted toward the channel center. The budgets of the Reynolds stresses have been computed. The significant differences are found between the budgets in this study and those in backward – facing step turbulence. The positive Reynolds shear stress $\overline{u'v'}$ is observed owing to the flow contraction just behind the ribbed.

Key words: Turbulent characteristic, wake region, rib, turbulent channel, vortices

1. Introduction

The ribs are often used to control the flow rate and to enhance the mixing in practical mechanical equipments. In the numerical studies of separated flows, the flow over a backward – facing step [4] , the ribbed channel [18] and the roughened channel flow [16],[14] are frequently employed. In particular, the flow through a two – dimensional backward – facing step is the most popular. The effect of step height was studied by [5]. The Kelvin-Helmholtz (K-H) vortices and the longitudinal vortices were observed behind the step [17]. Recently, the simulations for more practical configurations have been performed, for example, the flow over riblets or with one wavy wall [7].

In present work, the separation, the reattachment and also the contraction occur near and behind the ribbed therefore; the study of flow field with ribbed is useful to investigate the effects of the flow acceleration / contraction in the separated flow. In this study, the flow acceleration is defined as the positive streamwise mean velocity gradient $(\partial U/\partial x > 0)$ and the flow contraction $\partial V/\partial x \neq 0$ and / or $\partial V/\partial y \neq 0$, where U is the streamwise mean velocity and V the wall – normal mean velocity.

In the present work, numerical simulation of a turbulent channel flow with periodic two – dimensional ribbed has been carried out for $Re_{\tau 0}$=10-1500, where is the friction velocity defined later, the channel half width and the kinematic viscosity. The purposes of this study are to obtain the turbulent statistics for the development in turbulence modeling and to examine the relationship between the turbulent structures and turbulent statistics

behind the ribs.

2. Numerical model and validation
2.1 Governing equations

For steady incompressible turbulent flow, the Reynolds averaged equations for conservation of mass and momentum may be written as follows:

Continuity: $\dfrac{\partial u}{\partial x} = 0$ (1)

Momentum:
$$\frac{\partial}{\partial x}\left[uu - (v + v_t)\frac{\partial u}{\partial x}\right] = -\frac{1}{\rho}\frac{\partial P}{\partial x} + \frac{\partial}{\partial x}\left[v_t \frac{\partial u}{\partial x}\right]$$
(2)   where u is the velocity component x-direction, P is pressure, v is kinematic viscosity and v_t is the eddy viscosity obtained from the turbulence model.

Among several variations of widely used two-equation turbulence models, the low Reynolds-number (near-wall) properly resolve the complex flow behind around the ribs, following the work of [19]. This particular model is chosen because of its proven robustness and unambiguous near-wall treatment, two essential attributes in numerical modeling of separated flow about distributed ribs. The eddy viscosity is determined from two transport equations:

Turbulence kinetic energy (k):
$$(3)\quad \frac{\partial}{\partial x}\left[uk - \left(v + \frac{v_t}{2}\right)\frac{\partial k}{\partial x}\right] = P_k - \beta^* k\omega$$

$$Re_\tau = \frac{k}{\omega v}, \beta^* = \frac{9}{100} \cdot \frac{4/15+(Re_\tau/R_\beta)^4}{1-Re_t/R_\beta}, \quad R_\beta = 8 \quad (4)$$

Specific dissipation rate (ω):
$$(5)\quad \frac{\partial}{\partial x}\left[u\omega - \left(v + \frac{v_t}{2}\right)\frac{\partial \omega}{\partial x}\right] = \alpha \frac{\omega}{k}P_k - \beta\omega^2$$

$$\alpha^* = \frac{3/125 + Re_\tau/R_k}{1 + Re_\tau/R_k} \quad , \quad R_k = 6$$

$$\alpha = \frac{13}{25} \frac{1/9 + Re_\tau/R_\omega}{1 + Re_\tau/R_\omega} \frac{1}{\alpha^*} \quad , \quad R_\omega = 2.95 \quad , \quad \beta = \frac{9}{125}$$

$$P_k = v_t \left(\frac{\partial u_i}{\partial x_j} + \frac{\partial u_j}{\partial x_i} \right) \frac{\partial u_i}{\partial x_j}$$

Where P_k the production of turbulence kinetic energy and the eddy viscosity is is related to k and ω as:

$$(6) \quad v_t = \alpha^* \frac{k}{\omega}$$

2.2. Computational domain and boundary conditions

The configuration of the computational domain is shown in fig. 1a. A periodically repeating spatial unit with two-dimensional ribs is simulated. The periodic boundary conditions are employed in the streamwise (x) and spanwise (z) directions. The no-slip boundary conditions are used on all the walls. To ensure the grid resolution even close to the ribbed wall, a large mesh number is employed in the streamwise direction (see table 1). In the wall–normal direction, the density of the computational mesh is high at the height of the ribbed edges and near the walls (sees fig. 1b). The specific dissipation rate, ω is specified at the first grid off the solid surface and given a value $6v/(9\Delta n^2/125)$ where Δn denotes the normal distance from the wall [21].
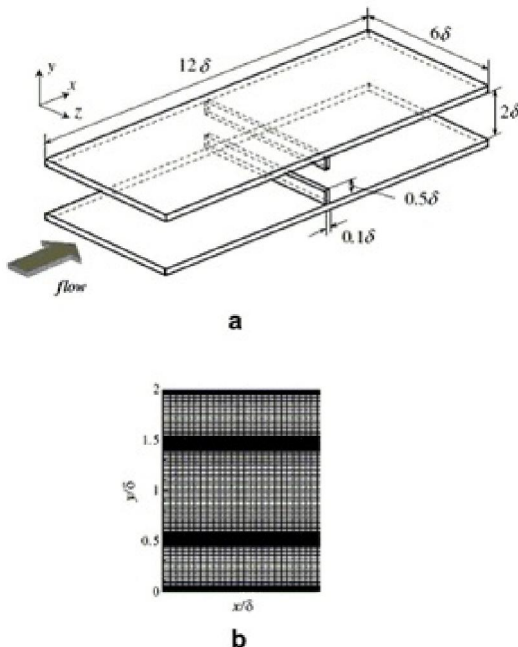

a

b

Figure.1.(a) configuration of the computational domain (b) computational mesh.

The ratio of ribbed height to channel height β is set to be 0.5, i.e., the distance between the wall and ribbed

edge h is 0.5δ in this study. The non – dimensionalized local friction velocity $u_\tau^*(-u_\tau/u_{\tau 0})$ for is shown in fig. 2. The streamwise –averaged friction velocity $\langle u_\tau \rangle_{ave}/u_{\tau n}$ is 0.26 in this case.
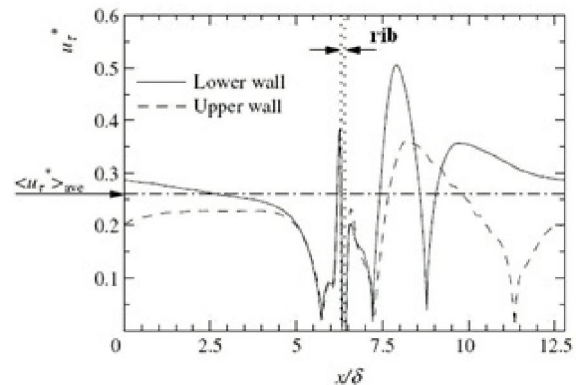

Figure.2. The non-dimentionalized actual friction velocity profiles for Reτ0=600.

2.3 Numerical solution procedure

The above equations are solved by a finite-volume method in an orthogonal body-fitted grid.

Second-order accuracy is assured by adopting the central differencing scheme throughout except for the convective derivatives that are discretized by the QUICK scheme. The continuity and the momentum equations, and the model equations for k and ω, are solved iteratively until convergence. The convergence criterion imposed in the calculation is that the sum of the residuals of mass source be less than 10^{-10}.

2.4. Validation tests

The major difficulty of model validation in the present case is the lack of adequately detailed experimental data for various rib shapes and block arrangements. In view of this, model validation is focused on two important features of the analysis: computation of separated flow and implementation of an orthogonal grid system.

The numerical model outlined above is validated against two test cases, namely, the backward facing step flow, and the square-ribbed channel flow, for which previous calculations provide a basis for comparison. Other researchers have also used these cases to validate their solution procedures and turbulence models. Therefore, it suffices to provide a very brief description of the results.

Fig.3. Backward facing step flow for $Re_h = 2800$ and $\delta_b/h = 1.1$ at $x/h = -3.8$: (a) streamlines and pressure contours; (b) c_f distribution along the channel. , For the backward facing step flow, calculations were performed in a solution domain $-3.8 < x/h < 80$ with

a grid $180 \times 80 \times 240$, in which 30 of the 80 grid points are distributed in the expanded region, for a Reynolds number (Re_h), based on step height h and the mean inlet velocity, of 2800. The inlet velocity profile is constructed to match the turbulent boundary layer of the experiment, i.e. $\delta/h = 1.1$. Fig. 3 shows the overall flow field and the friction coefficient along the wall downstream of the step. There is good agreement with the measurements of Vogel and Eaton (1985) .The computed reattachment length of 6.67h. These results provide a degree of validation of the numerical method and turbulence model.

Finally , the flow over the regularly distributed square ribs with $h/D_e = 0.1$ and $w/h = 7.2$ where D_e is the hydraulic diameter, is examined for $Re_{De} = 7,200$ .The mean velocity profiles at various cross-sections plotted in Fig.4 are seen to be in good agreement with the measured data of [9].
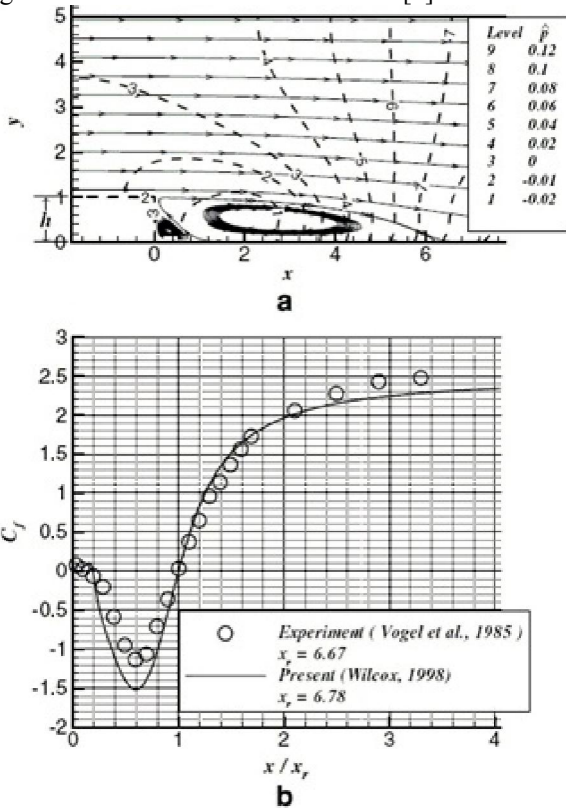

a

b

Figure.3. Backward facing step flow for Re_h=2800, (a)streamlines and pressure contours, (b)C_f distribution along the channel.

The discrepancy observed near the top surface of the rib, where the mean velocity attains a local maximum, was first suspected to be due to the insufficient grid resolution $(100 \times 80 \times 256)$. An additional calculation with much finer grid $(160 \times 150 \times 256)$ confirms that the solution is indeed grid-independent. The two-layer model of Chen and Patel (1988) may be the only exception that qualitatively shows the local maximum in

the mean velocity in that region. The results of the standard $k - \omega$ model with the wall function are shown in the Fig.4.for reference.
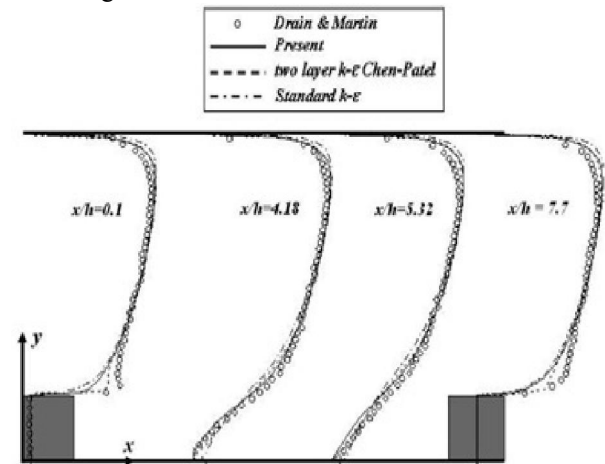

Figure.4. the mean velocity profiles at various cross-sections.

3.   Discussion about results
3.1.   Asymmetry phenomena and mean reattachment length

The streamlines of the mean flow for $Re_{\tau 0}$=20, 50, 300, 600, and 1500 are given in fig.5. The mean flow is asymmetry behind the ribbed in the cases of higher Reynolds numbers. These phenomena are referred to as the Coanda effect. The asymmetric direction depends on the initial flow field. We obtained the flow attachment to the upper and lower walls nearly with the same probability. In this study, the mean symmetric flow can be observed in the cases of $Re_\tau \leq 20$, i.e., $Re_b \leq 110$, and the mean flow becomes asymmetric in the cases of $Re_{\tau 0} \geq 30$ up to $Re_{\tau 0}$=1500, i.e., Re_b =7800.

In addition, we tested also an inlet- outlet boundary condition case (non- periodic) with a driver section which is a computational sub part to generate a fully developed turbulent channel flow for the inlet boundary condition [13]. The convective boundary condition is applied at the outlet boundary of the main part. Size of the used domain is $12\delta \times 2\delta \times 6\delta$ and the grid number is $256 \times 128 \times 256$ for the driver section. For the main section, the domain is $16\delta \times 2\delta \times 6.4\delta$ and the grid is the $512 \times 128 \times 256$. The ribbed is stationed at 4δ in the streamwise direction from the connecting plane between the sub and main parts. The time–averaged streamlines in the case of the inlet- outlet boundary condition are shown in (Fig.6).The mean flow becomes asymmetric as seen in the periodicity adds less effect on the asymmetry phenomena.

A large primary bubble is observed from the back-end of the rib to 9δ in the x-direction at the lower wall (Lr_1in Fig.5). In addition, a secondary bubble (B in Fig.5) generates to approximately 7.3δ in the x-direction

(see Lr_2 in Fig.5), i.e., 1.8h from the rib for $Re_{\tau 0}$=600. Le et la. (1997) reported that the length of the secondary bubble in the x-direction Lr_2 is 1.76h for backward-facing step flow. Therefore, the length of the secondary bubble is almost same in both the cases.

The reattachment length Lr_1 and the secondary bubble length Lr_2 are shown in (Fig.7). as a function of the bulk Reynolds number. In this study, the reattachment location is determined by the location of $\partial U/\partial y = 0$ at the wall.
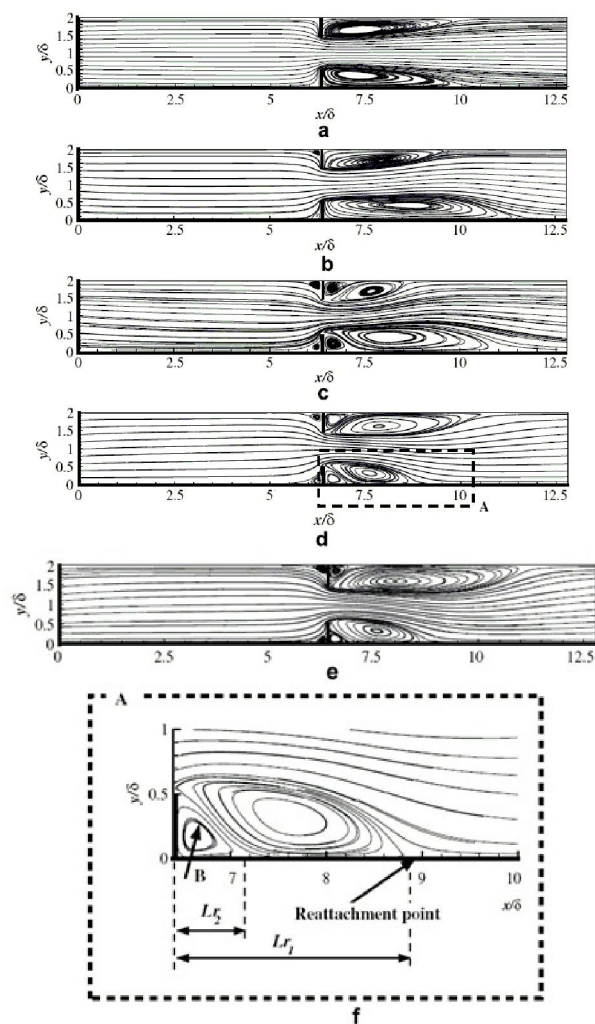

Figure.5. Averaged stream lines;(a) $Re_{\tau 0}$=20,(b) $Re_{\tau 0}$=50,(c) $Re_{\tau 0}$=300,(d) $Re_{\tau 0}$=600,(e) $Re_{\tau 0}$=1500,(f) enlarged view of the rectangular A in(d).
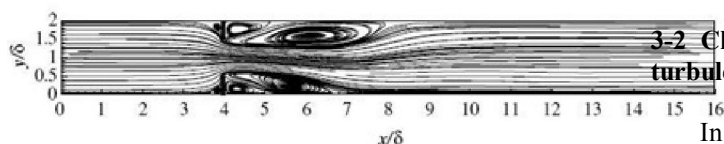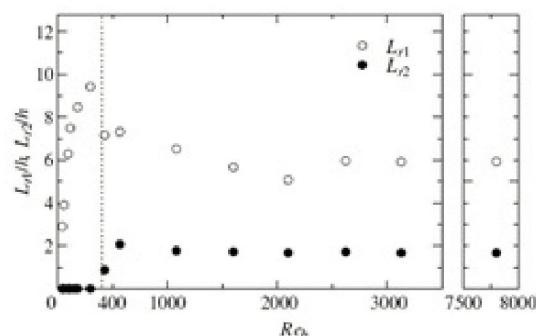

Figure.6. Averaged stream lines in the case of the inlet-outlet boundary condition.

The length Lr_1 is defined as the distance from the back-end of the ribbed to the reattachment location. Because the mean flow is asymmetric, the Lr_1 and the Lr_2 are obtained as an average of those on the upper and lower computational domain, i.e. the averaged reattachment point is calculated from (7).

$$1/2 \left(\partial U/\partial y|_{lower} + \partial U/\partial y|_{upper} \right) = 0 \qquad (7)$$

In the range of Re_b<400 range, the Lr_1 increases with increasing the Reynolds number. On the other hand, in Re_b>400 range, the reattachment length Lr_1 is characterized first by a sharp decrease and subsequently by a gradual one. These results are similar to those described in the case of the backward- facing step experiment [2]. One can clearly identify the laminar (Re_b<400), the transitional and the turbulent (400<Re_b<7800) ranges as implied by the shape of this profile.

(Fig.5). Reynolds number dependence of rectangular length Lr_1/h and secondary bubble length Lr_2/h from the back-end of the orifice.

The secondary bubble cannot be observed in the laminar region (Re_b<400). In the range of (400<Re_b<7800) ranges as implied by the shape of this profile.

The secondary bubble cannot be observed in the laminar region (Re_b <400). In the range of 400< Re_b <550, the secondary bubble length Lr_2 increases with increasing the Reynolds number and it becomes almost constant in Re_b>550 range. Therefore, the secondary bubble is generated in the transitional and the turbulent regime. In addition, the reattachment length Lr_1 at a higher Reynolds number (Re_b> 2000) is approximately 6h (=3δ) in this study. This corresponds roughly to the well- known length of 5-8h in the case of the turbulent flow over a backward–facing step [15].

3-2 Classification of wake region based upon the turbulent structures and statistics.

In this section, the relationship between the turbulent structures and the turbulent statistics in the case of $Re_{\tau 0} = 600$ are reported. In Fig.8 the wake region is classified based upon the budgets of the Reynolds stresses and the turbulent structures.

The region $\boxed{1}$ is the channel center near the rib. The Reynolds stresses and the turbulent energy in this region are much smaller than in other regions. The minimum value of the $\overline{u'u'}$ near the channel center is about 4.3 of the maximum value in the shear layer at $x_r/\delta = 1.0$.
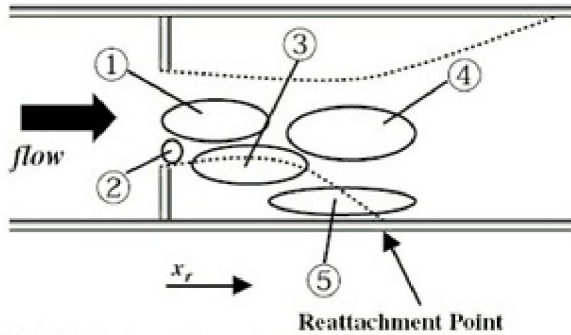

Figure.8. classification of the wake region.

Fig.9a and b show the streamwise evolutions of the streamwise mean velocity and the Reynolds stresses, respectively, where U^+ the non-dimensionalized is streamwise mean velocity at the channel center and $\overline{u_i'u_i'}$ indicates the Reynolds stresses on the centerline. The mean velocity increases in the streamwise direction in the range of $5.0 < x/\delta < 7.5$ by the flow acceleration through the ribbed.

The region $\boxed{2}$ for region $(y/\delta > 0.6)$, Reynolds stress $\overline{u'u'}$ exhibits the significant value and the mean velocity gradient $\partial U/\partial x$ is positive. This positive $\partial U/\partial x$ is caused by the flow acceleration through the ribbed. Therefore, the negative production of $\overline{u'u'}$ is due to the flow acceleration/contraction through the rib.
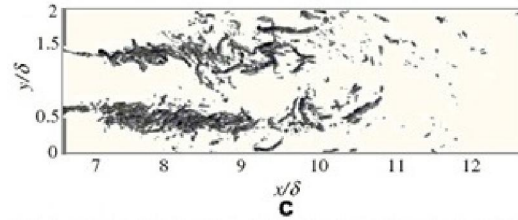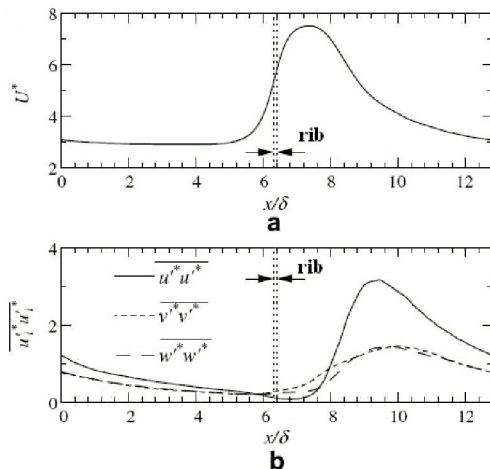

Figure.9.(a) Streamwise evolution of the streamwise mean velocity on y/δ =1line;(b) Streamwise evolution of the Reynolds stresses on y/δ =1line;(c) vortices behind the rib for $Re_{\tau 0}$=600 .

The region $\boxed{3}$ indicates the shear layer in the recirculation region. These profiles are characterized by the sharp peaks of the production and the large negative pressure strain for $0.5 < y/\delta < 0.75$ on the lower side. The peak production is caused by the large positive mean velocity gradient $\partial U/\partial y$. In the budgets of $\overline{u'v'}$ the $\partial U/\partial y$ also mainly contributes to the negative peak of the production term. In the shear layer, the pressure strain terms of $\overline{v'v'}$ and $\overline{w'w'}$ exhibit large positive values. Hence, the redistribution from $\overline{u'u'}$ to $\overline{v'v'}$ and $\overline{w'w'}$ is the dominant process in this region.

In the region $\boxed{4}$ ($x/\delta > 8$ and $0.5 < y/\delta < 1$ on the lower side of the channel), the turbulent diffusion term plays an important role. This term removes the turbulent energy from the shear layers and transports it to the channel center.

The contribution of the turbulent diffusion to the budgets becomes larger downstream in the center region of the flow (the center of the channel), i.e., $y/\delta = 1.0$, is not equal to the flow center because of the flow asymmetry. Thus, the turbulent diffusion contributes to the increase of the Reynolds stresses and the turbulent kinetic energy in the central region. Therefore, the turbulent diffusion adds more effects on the turbulent statistics at the channel center than in the case of the backward-facing step flow.

The region $\boxed{5}$ is located near the reattachment point (cf. the time-averaged reattachment length $L_{r1}/\delta \simeq 2.6$ on the lower side for $Re_{\tau 0} = 600$).

4. Conclusion

In the present study, we performed numerical simulation of turbulent channel flow with the periodic two-dimensional rib in various Reynolds numbers for $10 < Re_{\tau 0} < 1500$ $(40 < Re_b < 7800)$ and investigated the asymmetry phenomena. Mean reattachment length, vortex structures and the relationship between turbulence statistics and structures. The mean flow becomes asymmetric behind the rib because of the Coanda effect. In this study, this asymmetry phenomena can be observed for

$30 < Re_{\tau 0} < 7800,$ i.e., $180 < Re_b < 7800$. The Reynolds number dependence upon the reattachment length is similar to those described in the case of the backward-facing step experiment length is observed at $Re_b \simeq 400$. This is the transition from laminar to turbulence. The secondary bubble can be seen in the turbulent regime. The length becomes constant in the higher Reynolds number range.

The budgets of the turbulent kinetic energy and Reynolds stresses were calculated. We classified the wake region into five regions based upon the budgets of the Reynolds stresses and the turbulent structures. The several differences are found between the Reynolds stresses budgets in the present case and those in backward–facing step turbulence. The potential region is generated in the channel center near the rib. In shear layers just behind the rib, the Reynolds shear stress $\overline{u'v'}$ becomes positive owing to the effect of the flow contraction. In addition, the production terms of $\overline{u'u'}$ exhib its negative value near the ribbed edge. This is because of the flow acceleration/ contraction effects. These behaviors cannot be observed in the backward-facing step turbulence. At the shear layer in the recirculation region, the redistribution from $\overline{u'u'}$ to $\overline{v'v'}$ and $\overline{w'w'}$ is the dominant process. In the channel center at the recirculation region, the turbulent diffusion term transfers the turbulent energy from the shear layer to the channel center. In the wall vicinity of the recirculation region, the redistribution from $\overline{v'v'}$ to $\overline{u'u'}$ is promoted by the large scale splitting effect.

References

[1].Alleborn,N.,Nandakumar,K.,Raszillier.H.,Durst, F.,1997.Furher contributions on the two-dimensional flow in a sudden expansion. J.Fluids Mech.330 169-188.

[2]. Armaly,B.F., Durst, F.,Pereiar. J.C.F., Schonung B., 1983.Experimental and theoretical investigation of backward-facing step flow. J.Fluids Mech. 127,473-496.

[3]. Ashrafian, A.,Andersson, H.I.,Manhart, M.,2004 DNS of turbulent flow in a rodroughened channel. Int. J. Heat Fluid Flow25.373-383.

[4]. Avancha, R.V.R., Pletcher. R.H.,2002. Large eddy simulation of the turbulent flow past a backward-facing step with heat transfer and property variations. Int. J. Heat Fluid Flow 23,601-614.

[5].Chen.Y.T.,Nie.J.H.,Armaly,B.F.,Hsieh.H.T.,2006.Tur bulent separated convection flow adjacent to backward-facing step-effects of step height. Int. J. Heat Mass Transfer 49,3670-3680.

[6].Cherdron.W.,Durst,F.,Whitelaw.J.H.,1978.Asymmetr ic flows and instabilities in symmetric ducts with sudden expansion. J.Fluids Mech. 84,13-31.

[7].Choi,H.S.,Suzuki,K., 2005.Large eddy simulation of the turbulent flow and heat transfer in a channel with one wavy wall. Int.J.Heat Fluid Flow 26.681-694.

[8]. Comte.P..Lesieur,M.,Lamballais.E.,1992.Large-and small-scale stirring of vorticity and a passive scalar in a 3-D temporal mixing layer. Phys. Fluids 12.2761-2778.

[9]. Drain, L.E., Martin, S., 1985. Two-component velocity measurements of turbulent flow in a ribbed-wall flow channel. In: International conference on laser anemometry – advances and applications, Manchester, uk.<http:/tmdb.ws.tn.tudelft.nl/workshop7/case7-2/case 72d.html>.

[10].Durst.F.,Pereira.J.C.F.,Tropea,C,1993.The plane symmetric sudden-expansion flow at low Reynolds numbers.J.Flunds Mech.248,567-581.

[11].Fadlum,E.A., Verzicco,R,Orlandi.P., Mohd-Yusof. J.,2000.Combined immersed-boundary finite-difference. Methods for three-dimensional complex flow simulations.J.Comput.Phys.161,35-60.

[12].Fearn,R.M.,Mullin,T., Cliffe .K.A., 1990.Nonlinear flow phenomena in a symmetric sudden expansion.J.Fluids mech. 211,595-608.

[13].Inagaki,M.,Kondoh,T.,Nagano,Y.,2005.A mixed – time-scale SGS model with fixed model-parameters for practical LES.J.Fluids Eng.127.1-13.

[14].Krogstad,P.-A,Andersson,H.I.,Bakken,O.M.,Ashrafian,A.,2005. An experimental and numerical study of channel flow with rough walls.J.Fluids Mech.530, 327-352.

[15].Lesieur,M.,1997.Turbulence in Fludis.Kluwer Academic publishers. p.438.

[16].Nagano,Y.,Hattori,H.,Houra,T.,2004.DNS of velocity and thermal fields in turbulent channel flow with transverse-rib roughness. Int. j. Heat Fluid Flow 25.393-403.

[17].Neto,A.S., Grand,D., Metais,O.,Lesieur,M., 1993.A numerical investigation of the coherent vortices in turbulence behind a backward-facing step.J.Fluids Mech.256,1-25.

[18].Sewall. E.A.,Tafti.D.K.,Graham.A.B., Thole, K.A.,2006.Experimental validation of large eddy simulations of flow and heat transfer in a stationary ribbed duct. Int. J.Heat Fluid Flow 27,243-258.

[19]. Patel, V.C., Yoon, J.Y., 1995. Application of turbulence models to separated flow over rough surfaces.ASME J. Fluids Eng. 117,234-241.

[20].Stalio,E.,Nobile,E.,2003.Direct numerical simulation of heat transfer over riblets. Int. J.Heat Fluid Flow 24,356-371.

[21].Wilcox, D.C., 1998.Turbulence Modeling for CFD, second ed. DCW industries.

11/12/2011